Cross-correlated photon scattering during the photocycle of bacteriorhodopsin

József Czégé and Lou Reinisch
The Laser Biophysics Center and the Department of Radiology, Uniformed Services University, Bethesda, Maryland 20814 USA; and the Institute of Biophysics, Biological Research Center, Hungarian Academy of Sciences, Szeged, H-6701, Hungary

ABSTRACT Changes in the ultraviolet light scattering from a suspension of purple membrane fragments were detected during the photocycle of bacteriorhodopsin with a cross-correlation method. The scattered light intensity from a suspension of membrane fragments containing the protein bacteriorhodopsin was measured on a logarithmic time scale of 1 μs to 0.1 s at pH 4.6 after the photocycle was initiated with a polarized 532-nm laser flash. A simple model of curved sheets with positive and negative changes in the curvature is used to describe the observed light scattering changes. A detailed mathematical derivation of the model as well as the pictorial description are given. The changes in curvature of the membrane fragment are more than likely driven by the protein during the photocycle and are observed to have at least two time-resolved components, each changing the curvature of the fragment with an opposite sign.

1. INTRODUCTION

Bacteriorhodopsin (bR) is a photo-activated proton pump found in the purple membrane (PM) patches of the bacteria *Halobacterium halobium* (1, 2). The protein progresses through a sequence of intermediate steps during the photocycle, as evidenced by changes in the optical absorption spectrum (3). There have been attempts to link these absorption changes to significant rearrangements of the bR conformation: To date, studies indicate that the retinal chromophore does not move during the photocycle (4–8). Also, investigations of the protein side chains show no evidence for motion during the photocycle (9). However, some motion is probably involved in the photocycle because it can be influenced by the viscosity of the surrounding medium. When the membrane fragments are suspended in the higher viscosity medium of glycerol/water, the photocycle is slowed (10). In addition, the proton moves across the membrane during the photocycle. This motion has been directly measured by the protein electric response signal (PERS) method (11).

In earlier studies, the purple membrane fragments are observed by UV light scattering after photoexcitation with polarized light (12–14). Transient changes in the scattering cross-section for the membrane fragments are interpreted as small changes in the bending of the membrane fragments. Here we report on these transient changes in the scattering cross-sections with time resolution of 1 μs. We find the dynamics of the membrane to be much more complicated than earlier interpretations showed. The fragments undergo forced changes in curvature in opposite directions with different time scales during the photocycle.

The mathematical derivation of the expected scattering changes from the bent sheet model is presented in Appendix A. We expand upon earlier derivations (12–14) and also present a treatment of the scattering changes due to absorption changes in the sample in Appendix B.

2. MATERIALS AND METHODS

Purple membrane fragments are isolated from the strain ET1001 of *Halobacterium halobium* according to the procedure of Oesterhelt and Stoeckenius (15). The samples are graciously provided by Dr. Zsolt Dancsházy. The samples are suspended in 10 mM potassium biphthalate buffer. The concentration of the bR in the samples is determined by measuring the absorption spectrum (Spectronic 1201, Milton Roy Co., Rochester, NY) in a 1-cm cuvette. The samples are very stable and show no signs of aggregation with the low salt concentration. No settling of the PM fragments is observed, even after 1 wk of storage. The extinction coefficient of bR at 568 nm has been reported to be 63,000 $cm^{-1}M^{-1}$ (16). Using our measured absorption spectra, the extinction coefficients for the bR_{568} at 325 nm is ~4,500 $cm^{-1}M^{-1}$ and at 532 nm is 44,000 $cm^{-1}M^{-1}$.

Samples of the PM suspended in agar gel are made by dissolving agar (Bactoagar, Difco Laboratories, Detroit, MI) into water (2.5% agar) at 80°C. The gel is cooled to about 40°C before the concentrated PM suspension is added and mixed thoroughly. The sample is then allowed to gel at room temperature in a cylindrical cell. The pH is controlled by immersing the gelled sample into a 10-mM potassium biphthalate buffer solution. The cylindrical gel sample is allowed to equilibrate with the buffer solution overnight. Tests of this method were made agar gel samples (no PM) equilibrated in copper sulfate solutions. Visual inspection showed that copper sulfate was able to diffuse into the gel within a couple of hours. Even though the smaller salt ions diffuse in rather rapidly, we have observed no loss of bR from the gel samples, even after several months of storage in the buffer solution.

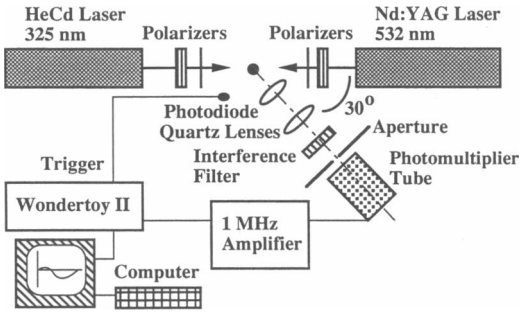

FIGURE 1 A block diagram of the experimental setup. The frequency doubled, Q-switched Nd:YAG laser excites the photocycle with 1.5-mJ pulses at 532 nm (30-ns pulse length). The polarization of the laser is selected with a combination Glan–Taylor prism and thin film polarizer. The HeCd laser (325 nm, 7 mW) illuminates the cylindrical sample cell from the opposite direction. The polarization is selected with a combination of a Glan–Thompson prism and a thin film polarizer. The sample cell is held in an index matching goniometer at room temperature. The scattered light is collected and focused onto a 1-mm aperture in front of the photomultiplier tube (PMT) with two quartz lenses. An interference filter blocks the room light and most of the 532 nm light from entering the PMT. The PMT has a 1-kΩ anode resistor, and the signal is amplified with a DC to 1 MHz amplifier. The digitizer runs on a logarithmic time base and is triggered with an optical diode. Subsequent data storage and analysis are performed with the computer.

The geometry of the scattering system with a 30° scattering angle is shown in the block diagram of the experiment in Fig. 1. The monitoring light is the 325-nm line (7 mW) from a HeCd laser (Liconix, Sunnyvale, CA). The polarization is selected using a quartz Glan–Thompson polarizer (Newport Corp., Fountain Valley, CA) and a membrane polarizer (Oriel Corp., Stratford, CT). The exciting flash is from a frequency doubled, Q-switched Nd:YAG laser (attenuated to 1.5 mJ/pulse) at 532 nm (Quantel Int., Santa Clara, CA). The Nd:YAG laser has a 10-Hz repetition rate with an average power of 15 mW. Repetition rates of 5 and 2 Hz are also used to ensure that heating is not affecting the measurements. The polarization of the pulsed laser is selected with a quartz Glan–Taylor polarizer (Newport Corp., Fountain Valley, CA) and membrane polarizer to avoid changes in the beam direction when selecting different polarizations. Detection is made by a photomultiplier tube (type 9863, Thorn EMI Gencom Inc., Plainview, NY). The signal is amplified (AM 502, Tektronix Inc., Beaverton, OR), then digitized with a logarithmic time base (Wondertoy II, University of Illinois, Urbana, IL) and processed by computer (WGS 6300, AT&T, Morristown, NJ). The PM suspensions are held in 10 × 75 mm cylindrical test tubes of borosilica glass.

The percent changes in the scattered light have two components: one scales with bR concentration, the second is independent of bR concentrations (see Appendix B). To separate the two signals, the experiment is performed at a number of concentrations. At each concentration we measure the changes in the scattered light at 42 equally spaced points on a logarithmic time axis. We then plot the changes in the scattered light as a function of the bR concentration for each of the 42 time points. These data are then fit to 42 independent straight lines using a least squares routine. The 42 slopes and intercepts of the fits give the scattering changes proportional to the bR concentration and the scattering changes independent of the bR concentration, respectively.

3. RESULTS

Fig. 2 *a* shows the transient changes in the scattered light measured at 325 nm during the bR photocycle. The figure plots the percent change in the scattered light versus the time after the visible laser flash on a logarithmic time scale. The four curves show the scattering measured using vertically and horizontally polarized monitoring (325 nm) light (I_V and I_H) and vertically and horizontally polarized exciting (532 nm) light (E_V and E_H).

As a control, we repeat the above experiments with the bR fixed in 2.5% agar gel. In the gel, the membrane motion is constrained. The transient scattering signals are

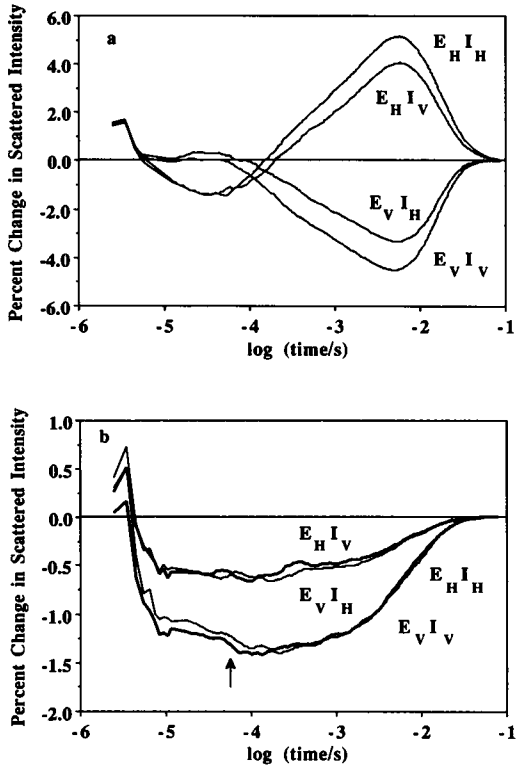

FIGURE 2 (*a*) The observed scattering changes from a 5-μM suspension of bR in membrane fragments in water at room temperature. The excitation at 532 nm is either vertically or horizontally polarized (E_V or E_H). The scattering is measured at 325 nm with either vertically or horizontally polarized probe light (I_V or I_H). The four curves are labeled for the polarizations used. The initial deflection of the data (faster than 8 μs) is from laser light leaking into the PMT. (*b*) The observed scattering changes from an ~20 μM suspension of bR in membrane fragments in a 2.5% agar gel. Here the membrane fragments are constrained and unable to change their curvature. The scattering changes are induced by changes in the absorption of the sample at 325 nm during the photocycle. The polarizations on the monitoring and scattering light are indicated. The bold lines are used for the horizontal excitation (E_H); the thin lines are used for the vertical excitation (E_V). The arrow locates the slight "kink" observed in the curve.

shown in Fig. 2 *b*. The smaller signal observed here is due to changes in the absorption of the 325-nm light that also occur during the photocycle. These absorption changes are small and slightly distort the measured scattering.

Previous studies performed on PM fragments in this same brand of agar gel indicate that the photocycle is not significantly altered by the gel (9). We therefore feel that Fig. 2, *a* and *b*, can be compared qualitatively. However, a direct quantitative comparison is difficult. The concentration of the bR in the two samples must be identical. In addition, the agar scatters much more light than water. So, the intensity of the exciting laser flash is slightly attenuated in the gel sample. The additional scattering from the agar will cause an artificial decrease in the amplitude, because we measure the percent change in scattering.

The scattering changes due to changes in the chromophore can be separated from the scattering changes due to a change in membrane cross-section by diluting the sample. The true fractional scattering changes due to cross-section changes will remain constant (as long as the membrane fragments remain the dominant scattering center) and the changes in scattering due to changes in the chromophore will scale with the chromophore concentration, Eq. B10. We measure the scattering from a sample at 5.0 μM concentration. We then dilute the suspension to 2.5, 1.25, and 0.63 μM. For each concentration the transient scattering is measured. The scattering transients at each time point for the four samples are fit as a linear function of the chromophore concentration. The scattering changes independent of the chromophore concentration are shown in Fig. 3 *a* (the intercepts of the linear least squares fit). Also shown in Fig. 3 *a* are the changes that scale linearly with the chromophore concentration. These are the scattering changes induced by absorption changes. The linear least squares fits for several time points are shown in Fig. 3 *b*. The linear approximation outlined in Appendix B appears to be valid for these data.

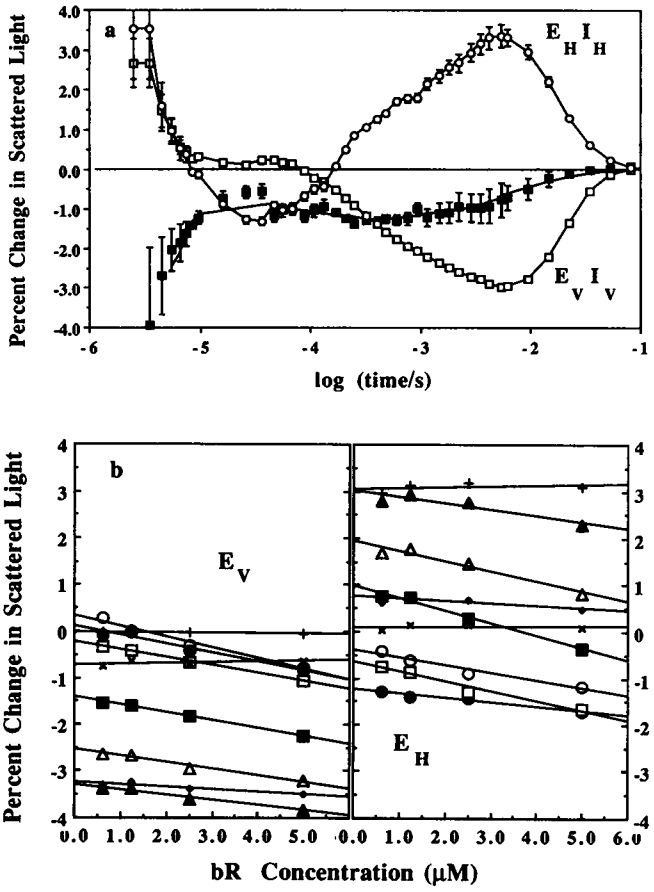

FIGURE 3 (*a*) The scattering is measured from a suspension of 5.0 μM bR. The sample is diluted to 2.5, 1.25, and 0.63 μM. The scattering is measured for each sample. The scattering for each time point is then fit with a linear least squares method as a function of the chromophore concentration. The percent changes in the scattered light due to membrane fluctuations should be independent of chromophore concentration. These concentration-independent scattering changes (intercepts from the least squares fit) are shown as open points. Error bars are determined from the residuals of the least squares fit. Scattering changes for the two polarizations ($E_H I_H$ and $E_V I_V$) are shown. Scattering changes that scale with chromophore concentration (slopes from the least squares fit) are shown as solid points. Error bars are determined from the residuals of the least squares fit. Scattering from times faster than 10 μs are influenced by the scattered light at 532 nm leaking into the PMT. (*b*) Demonstrations of the linear dependence of the scattering from suspensions of PM fragments. The percent change in scattering is plotted as a function of the bR concentration for 9 equally spaced log(time) points for horizontal and vertical excitation (E_H and E_V, respectively). The lines are least squares fits to the data. The time points are: (○) 10 μs; (●) 30 μs; (□) 100 μs; (■) 300 μs; (△) 1 ms; (▲) 3 ms; (+) 10 ms; (♦) 30 ms; (×) 0.1 s.

4. DISCUSSION

The surface of the PM fragment is asymmetrically charged (17, 18). The most energetically favorable configuration for a flexible membrane with a fixed asymmetric charge distribution is curved. Therefore, it is not unreasonable to assume that the PM fragment is curved. The changes in the scattering cross-section of the PM fragments during the photocycle of the bR can be explained by changes in the curvature of the membrane fragments.

The membrane fragments are thin sheets, reported to be 4.9 nm (19) and 4.35 nm (20) thick and on the order of 1 μm in diameter (21). We also note that the effective diffusion diameter for the fragments has been reported to be slightly smaller. Arrio et al. finds a PM fragment to have an effective diameter near 0.3 μm (22). The curved surface of the fragment could account for some of this difference. Also, the handling of the PM fragments could

have an influence on their size. It is possible that the larger fragments are torn with the shear forces of the suspending medium.

The dipole of the retinal groups, arranged in symmetric trimers, are essentially parallel (20°) to the membrane surface (23). It is important to recall that the visible laser flash will interact with the retinal dipole. When the light polarization is parallel to the retinal dipole, it is preferentially absorbed. The ultraviolet light scatters off of the membrane surface. The orientation of the membrane fragments with respect to the excitation and probe light is, therefore, important. There are essentially three broad classes of membrane orientation possible. These are shown in Fig. 4 and labeled as class 1, 2, and 3. While it is not exact to categorize all membrane orientations by these three classes, we can use them to qualitatively explain the scattering transients (see Appendix A).

We first consider excitation with horizontally polarized light (E_H). In Fig. 4, this light travels across the page with the polarization vector out of the paper. This polarization will primarily excite those PM fragments in class 1 and class 2 (see Appendix A for a mathematical verification). In these two orientations, the angle between the membrane surface and the incident horizontal polarization is a minimum. Therefore, the excitation of the retinal timers in the membrane is maximal. The scattering from the membrane is maximized when the surface normal is parallel to the scattering vector. The scattering vector bisects the angle formed by incident light and the scattered light. For this experiment, the scattering vector is out of the paper and nearly perpendicular to the paper. It can be seen from Fig. 4 that scattering will decrease when the curvature of the class 1 and 2 orientations decreases. Likewise, the scattering will increase as the curvature increases for the class 1 and 2 orientations. See Appendix A and references 12–14 for the mathematical treatment of this model.

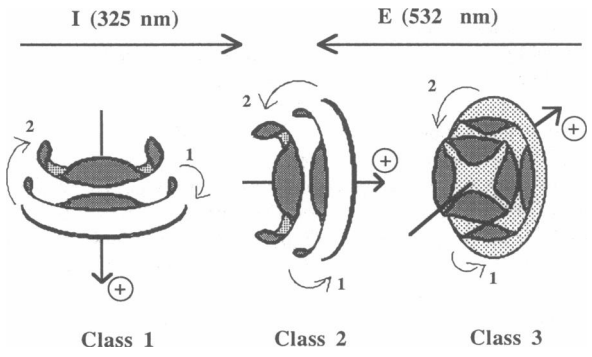

FIGURE 4 The three classes of PM orientation are shown. The 532-nm light travels from right to left across the page; the 325-nm light travels from left to right. The middle membrane in each class is the initial configuration. The membranes decrease the amount of curvature (*1*) and then increase the curvature (*2*). Finally, they relax to the original configuration. For simplicity, cylindrical curvature about two perpendicular axis is shown. In the actual PM it is probably more complicated. Also, the curvature changes are exaggerated for illustration purposes. The arrows through the membrane fragments show the direction of the proton pump with respect to the membrane curvature for pH 4.6. Class 1 and 2 PM fragments are primarily probed with horizontally polarized excitation. Class 3 PM fragments are primarily probed with vertically polarized excitation (see Discussion in the text).

We observe in the experimental data an initial decrease in the scattering, then an increase in the scattering of the probe beam after the excitation with horizontally polarized light. This implies first a reduction in the curvature, followed by an increase in the curvature of the membrane fragments after photoexcitation. One might descriptively term this a "flapping" of the PM after photoexcitation (see Fig. 2 *a* of reference 22 for a micrograph suggesting PM flapping).

Excitation with vertically polarized light (E_V) will excite those membranes with orientations in class 2 and class 3. However, most of the scattering of the probe beam will be due to the class 3 orientation of PM fragments. So, we neglect the class 2 orientation and take into account only the class 3 orientation. This may seem to be an oversimplification of a complicated system, but careful mathematical analysis has been performed and supports the simple picture presented here (see Appendix A and references 12–14). The PM fragments excited with vertically polarized light will therefore decrease in scattering cross-section when the bending is increased. Likewise, they will increase in scattering cross-section when the bending is decreased (or the "flaps" are open).

This picture is consistent with the measured scattering. After photoexcitation the membrane initially reduces its curvature. This leads to an increase in scattering when excited with vertically polarized light. The reduced curvature is then followed by increased curvature. This leads to a reduction in the scattering of the probe light by the class 3 orientation (those excited with E_V).

This simple model explains the observed scattering data very well. The transient scattering has a different sign depending upon vertical or horizontal excitation polarization. This experimental result may be very disturbing at first. Upon careful analysis we find that the scattering changes in opposite directions for vertical and horizontal follows directly from the model (changing the membrane curvature).

Of course, the actual situation has additional complications. It is possible for the membranes to rotate during the experiment. The rotation of the entire fragment during the course of these experiments will decrease the signal size. Photoselection experiments using polarized light indicate that the PM fragment rotation is significantly slower than the period of the photocycle (9). Additionally,

the PM fragments require orientation for the PERS signal. In these measurements, the suspension of PM fragments retains its orientation for ~0.1 s after the orientation electric field is turned off (24).

In this discussion, we have thus far assumed that the dipole moment interacts only with the pulsed laser; there is no absorption of the UV light by the sample. This is not strictly true. There is a slight increase in absorption of the UV light by the PM when the protein undergoes its photocycle. The changes in absorption will cause apparent changes in the scattered light. The changes in the scattering signal due to absorption changes can be measured by putting the membrane fragments into a gel, where they are constrained and unable to change their curvature. The changes in scattering due to absorption changes measured at 325 nm are consistent with known rates for the bR photocycle. A slight "kink" in the scattering in the gel sample due to absorption changes (Fig. 2 *b*) is seen at ~80 μs corresponding to the L $\rightarrow$ R transition. This kink is more obvious in samples with a higher concentration of bR. Also, the final decay of the absorption-induced scattering change is consistent with 1.5–3 ms time for the O $\rightarrow$ bR transition measured with PM in a water suspension (2, 24).

In Fig. 4 the direction of the proton pump is shown with respect to the membrane curvature. The initial reduction in curvature is shown, then the increase in curvature, finally the fragment returning to its initial state of curvature. The initial change from a curved membrane to a more flat membrane is a driven reaction. The exact time of the initial change is difficult for us to determine with our data. The 1-μs resolution of our A/D converter, and the leakage of the pulsed laser light into the photomultiplier distorts the data faster than ~8 μs. Needless to say, the first change in curvature happens very quickly. It probably takes place or starts within the 2–3 μs time known for the K $\rightarrow$ L transition. The change in curvature is probably a delayed response to an impulse force for this initial fast transition.

Subsequently, the membrane is driven to a more curved state with a time constant near 80 μs. The 80-μs time corresponds with the observed absorption "kink" in Fig. 2 *b*. Also, this corresponds well with the time for the L $\rightarrow$ M transition. We know this is not a spontaneous relaxation of the membrane, because the spontaneous relaxation occurs much slower. A relaxation is seen at the end of the kinetics, and it is, in fact, slower than the photocycle.

Finally, after the photocycles of the many protein molecules held in each PM fragment are complete, the membrane relaxes to its initial state with a very nearly single exponential decay time. In Fig. 5 we show the absolute value of the percent change in scattering on a logarithmic scale versus linear time. Here, the exponential nature of the decay is very apparent. In addition, the relaxation differs slightly for vertical and horizontal excitation (E_V and E_H). The vertical excitation scattering change decays with a rate of 108 ± 4 s^{-1}. The horizontal excitation scattering change decays with a rate of 71 ± 2 s^{-1}. The values of these relaxation rates, of course, depend upon the handling of the sample and the PM fragment size. Yet, the PM fragments excited with vertically polarized light always shows a faster decay than the PM fragments excited with horizontally polarized light. Further investigations are needed to understand this difference. We note that the different polarizations view the membrane fragments and the relaxation differently (see Fig. 4). It is not unreasonable to see different relaxation times. It is also possible that the relaxation time could be slightly influenced by the rotational time of the membrane fragments. Recall that the characteristic time of the rotation is on the order of 0.1 s or longer for PM (24). Further work in this area is clearly needed.

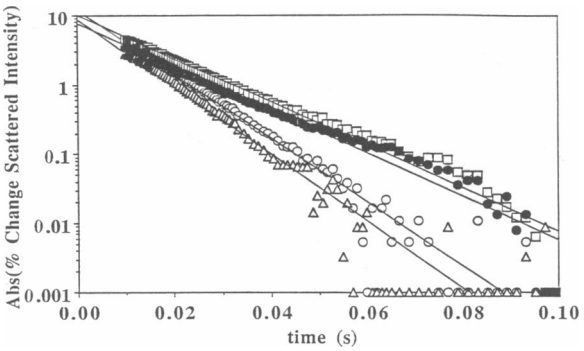

FIGURE 5 The absolute value of the percent changes in scattering on a logarithmic scale vs. linear time (same data as Fig. 2), for times >8 ms. (○) $E_H I_H$; (△) $E_H I_V$; (□) $E_V I_V$; (●) $E_V I_H$. Straight lines show the least squares fit to the data with rates of 105, 111, 71, and 71 s^{-1}, respectively.

The reduction in membrane curvature followed by an increase in curvature before the membrane relaxes to its initial state is an exciting result. Measurement of charge movement with the PERS technique has indicated for many years that the charge first moves in one direction and then reverses direction during the photocycle of bacteriorhodopsin (11, 24). In fact, a slingshot model for the proton pump of bR was introduced. In the PERS experiments, the first "backward" motion of the proton occurs in several fast steps. The slowest step of the backward motion occurs in 2–3 μs. We propose a simple model where the backward motion of the protons causes the PM fragment to flatten because of electrostatic repulsion (see Fig. 6). The subsequent forward motion of the proton measured with PERS follows in several steps. These steps correlate with the intermediates of the bR photocycle measured with optical absorbance changes.

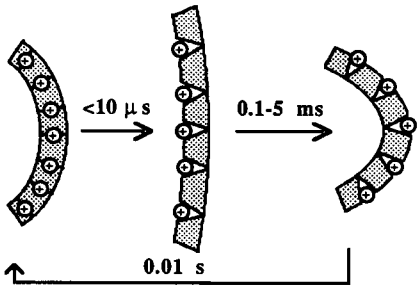

FIGURE 6 A simple model that correlates the motion of the proton as measured with the PERS method to the changes in curvature seen with light scattering. The membrane fragment is initially curved with the proton located somewhere inside PM. The proton initially moves backwards within a few microseconds. This causes the membrane to flatten from the electrostatic forces. The proton is then pumped across the membrane. The charges on the opposite side of the membrane surface cause an increased bending of the membrane. Finally, the system relaxes to the initial state. The times shown on the model are approximate.

According to the model shown in Fig. 6, the forward moving protons will cause an increase in the membrane curvature. Our simple model correlates well with the PERS measurements, but it clearly needs experimental verification. Yet, the correlations with the direction of proton motion and changes in curvature are worth noting.

The membrane bending is significant in the study of bR. The membrane motion observed here indicates a link between the function of bR and the dynamics of the membrane. Understanding the external controls on a protein is an important aspect in understanding the function of a protein. Additionally, if the correlation between the proton motion and the bending (as mentioned above) is justified, then the membrane motion is an additional probe to the motion of the proton. Additional work is in progress to measure the fast changes in the bending of the membrane fragments as a function of the pH and the viscosity of the suspending medium. This should give us new insight to the function of bR.

APPENDIX A

We present here the mathematical analysis of the excitation and scattering process. For clarity, we will treat the excitation and scattering separately. The polarized excitation light interacts with the chromophore transient dipole moment (the retinal) and selects specific orientations of PM fragments. The scattering process is from the membrane and will change with the membrane cross-section.

To analyze the excitation process, recall that the probability of exciting a chromophore with a transition dipole moment μ is given by

$$w \sim \mu^2 \cos^2 \phi, \tag{A1}$$

where ϕ is the angle between the direction of the polarization of light and the transition dipole moment. The dipoles of the retinal groups are arranged in symmetric trimers as shown in the coordinate system in Fig. 7 *a*. The membrane normal, **n**, is along the *z*-axis. The incident exciting light has a polarization vector, **p**, where ω is the angle between **n** and **p**. The retinal dipoles are shown as three symmetric **r** vectors at an angle δ from the membrane normal. Accounting for the trimer arrangement of dipoles, Eq. A1 now becomes

$$w \sim \mu^2 \left[\cos^2 \delta \cos^2 \omega + \frac{1}{2} \sin^2 \delta \sin^2 \omega\right]$$
$$= \mu^2 \left[\frac{1}{2} \sin^2 \delta + \frac{1}{2}(2 - 3 \sin^2 \delta) \cos^2 \omega\right]. \tag{A2}$$

The membrane is not flat, but curved with an angle Ψ_o as shown in Fig. 7 *b*. Therefore, the value of $\cos^2 \omega$ must be averaged over the membrane. In the case of spherical curvature, we note that

$$\langle \cos^2 \omega \rangle = \frac{1}{2\pi(1 - \cos \Psi_o)} \int_0^{2\pi} d\phi \int_0^{\Psi_o} d\theta \sin \theta \cos^2 \omega$$
$$= \frac{1}{3}\left[1 + \cos \Psi (1 + \cos \Psi)\left(1 - \frac{3}{2} \sin^2 \omega_0\right)\right], \tag{A3}$$

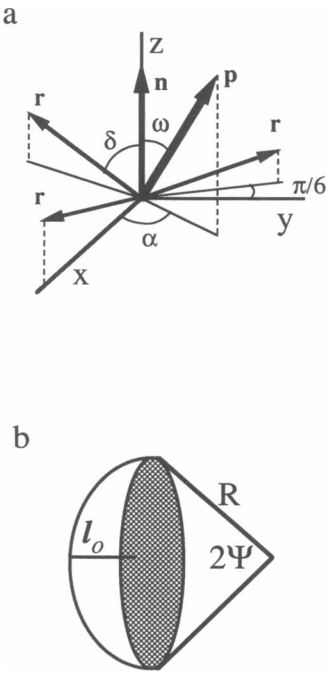

FIGURE 7 (*a*) The three symmetric dipole moments of the bR trimer are shown as **r** vectors. The membrane normal, **n**, is along the *z*-axis. The angle between **r** and **n** is δ. The incident light has a polarization along the **p** vector. The angle between **p** and **n** is ω. The symmetry of the three **r** vectors makes the result of the dipole interaction term, Eq. A2, independent of the angle α. (*b*) A schematic of a spherically bent membrane fragment, with radius of curvature, R and angle of curvature 2Ψ. The thickness of the membrane in the radial direction (the l-direction), is l_0.

where ω_0 is the angle between $\mathbf{p}$ and $\mathbf{n}$ at the center of the membrane fragment. The important results of Eqs. A2 and A3 may not be apparent. There are three broad classes of membrane orientation possible. These are shown in Fig. 4 and labeled as class 1, 2, and 3. Horizontally polarized exciting light (E_H) travels across the page in Fig. 4, from right to left with the polarization vector out of the paper. Class 1, 2, and 3 will correspond to $\omega_0 = 90$, 90, and 0°, respectively. We allow δ to be nominally 70°, then Eq. A2 is maximized for class 1 and 2 orientations and minimal for the class 3 orientation. With similar arguments, one can see that vertically polarized exciting light (E_V) will primarily excite the PM fragments in class 2 and 3. Of course, in the suspensions all orientations are possible, and categorizing each membrane into one of the three classes will not yield exact solutions. We, therefore, integrate over all orientations when making our calculations.

Due to the membrane fragment size, we can use the Rayleigh–Debye approximation to describe the scattering (25). The intensity of the scattered light is determined from the form factor P:

$$P(\theta) = \frac{1}{V^2}\left|\int_V \exp(ihs)\, dV\right|^2, \qquad \text{(A4)}$$

where θ is the scattering angle and V is the volume of the scattering particle. The coefficient $h = (4\pi/\lambda)\sin(\theta/2)$, where λ is the wavelength of the scattered light, and $|s|$ is the length of the projection of the position vector of an arbitrary point on the membrane to the direction of the scattering vector (25).

The scattering cross-sections are proportional to the form factor according the following relations

$$\sigma_\perp \sim V^2 P(\theta), \quad \sigma_\parallel \sim V^2 P(\theta)\cos^2\theta, \qquad \text{(A5)}$$

where $\sigma_\perp$ and $\sigma_\parallel$ are the scattering cross-sections when the incident light is polarized perpendicular and parallel to the scattering plane, respectively (25). The scattered light is proportional to the scattering cross-section.

The integral in Eq. A4 can be expanded for the case of spherically bent surfaces

$$P(\theta, \epsilon) = \left|\frac{1}{l_0}\int_0^{l_0} J_0(h\rho\sin\epsilon)\exp(ihl\cos\epsilon)\, dl\right|^2, \qquad \text{(A6)}$$

where J_0 is the zero order Bessel function, and $\rho = \sqrt{R^2 - (R-l)^2}$. The angle ϵ is between the membrane normal and the scattering vector, s. The length, l, is across the membrane with a total thickness of l_0. The scattered light intensity is proportional to the form factor in the case of constant particle volume, Eq. A5. Using the coordinate system shown in Fig. 8, the exciting light at 532 nm is incident from the $-x$ direction. The probe light at 325 nm is incident from the $+x$ direction. The angle θ is 30° in our experiments. Class 1 membranes will have $\epsilon = 90°$; class 2 will have $\epsilon = 75°$; class 3 will have $\epsilon = 15°$.

In the case of vertically polarized exciting light (E_V), class 2 and 3 membrane fragments are primarily excited. From Eq. A6, we find that the scattering form factor is orders of magnitude larger for the class 3 membrane fragments compared to the class 2 fragments. We therefore only consider the class 3 fragments. In Eq. A6, ϵ is not a single value, but varies due to the curvature of the membrane. Increasing the curvature will increase the range of ϵ. Analysis of Eq. A6 shows a decrease in the form factor with an increase in curvature for $\epsilon < 30°$ for 0.25 μm^2 membranes (12). This is an agreement with the pictorial argument presented in Fig. 4.

Horizontally polarized exciting light (E_H) will excite class 1 and 2 membrane fragments. When $\epsilon > 60°$, the scattering form factor increases with increased curvature for the 0.25 μm^2 membranes (12). This is also in agreement with the pictorial argument presented in Fig. 4.

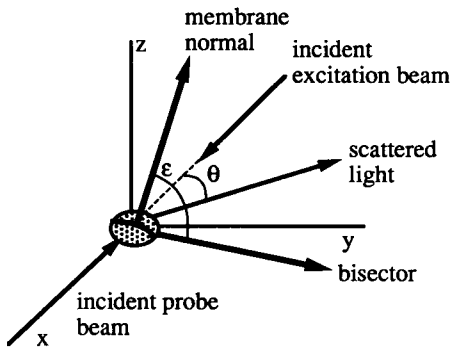

FIGURE 8 The orientation of the PM fragment is defined with the incident probe beam coming from the $+x$ direction, and the incident excitation beam coming from the $-x$ direction. The xy plane is the scattering plane, with the scattering angle, ϕ, measured from the $-x$ axis. The membrane normal forms an angle ϵ with the bisector of the compliment of angle θ.

APPENDIX B

We treat here the change in the scattering transients as a function of the chromophore concentration. The chromophore concentration will change the observed scattering signal via two major effects: It will attenuate the exciting light that reaches the center of the sample. Secondly, if the chromophore changes its absorption at the probe beam wavelength, then the amount of scattered light making it out of the sample and to the detector will also be changed by the absorption transients. We account for both of these effects in the following.

A schematic of the situation is presented in Fig. 9. The excitation beam enters the sample from the top. The volume of the illuminated sample imaged into the PMT has a length l and has a width of w. The probe beam enters from the bottom. Given that c_{pm} is the concentration of purple membrane fragments, then the amount of light scattered (dI_{sc}) from the volume element dV is

$$dI_{sc}(t) = I_m(\xi, t)\sigma(\xi, t)c_{pm}dV. \qquad \text{(B1)}$$

I_m is the intensity of the probe beam a distance ξ into the sample and at the time t. The scattering cross-section of the PM fragments is σ, with ξ and t denoting position and time, respectively. This scattered light must pass through a pathlength ρ of the suspension to reach the detector. So, it is attenuated and the scattered light is now

$$dI_{sc}(t) = I_m(\xi, t)\sigma(\xi, t)c_{pm}\exp[-\eta_{325}(\xi, t)\rho c_{bR}]\, dV. \qquad \text{(B2)}$$

Here, c_{bR} is the concentration of the bacteriorhodopsin. Also, η is the nondecadic absorption coefficient of bR. The subscript gives the wavelength. At time $t = 0$, the scattered light for the volume element can be written as

$$dI_{sc}(t = 0) = I_0\sigma^0\alpha c_{bR}\exp[-\eta^0_{325}c_{bR}(\xi + \rho)]\, dV. \qquad \text{(B3)}$$

Both $\sigma(\xi, t)$ and $\eta(\xi, t)$ depend upon ξ and t due to the attenuation of the excitation light as it passes through the sample and the changes in the

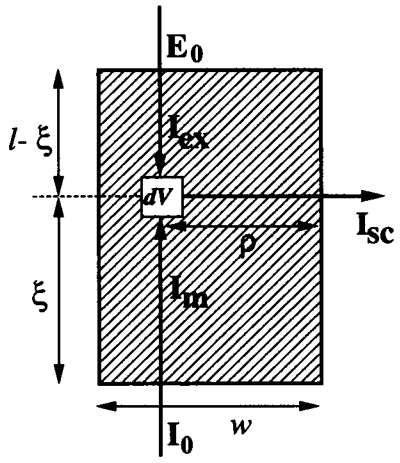

FIGURE 9 The volume of the PM suspension imaged onto the PMT. The incident excitation light, E_0 enters from the top of the page. The probe beam, I_0 enters from the bottom of the page. The scattered light, I_{sc}, is from volume element dV, and must be integrated over the entire volume. Both the excitation and probe beams are attenuated by the sample absorption. The probe beam will experience a time-dependent attenuation due to the change in the absorption of the sample as it goes through the photocycle. Additionally, the scattered light is attenuated as it passes out of the suspension. The full analysis is presented in Appendix B.

bR absorption during the photocycle, respectively. To simplify the notation, we use $\eta^0 = \eta(\xi, t = 0)$ and $\sigma^0 = \sigma(\xi, t = 0)$. At time $t = 0$, all the bR is in the ground state and the absorption and scattering cross-section is not a function of ξ. In Eq. B3 we have also used $\alpha c_{bR} = c_{pm}$ to simplify the notation. We can explicitly identify the scattering cross-section and absorption as

$$\sigma(\xi, t) = \sigma^0[1 + s(t)I_{ex}(\xi)] \tag{B4a}$$

$$\eta(\xi, t) = \eta^0 + k(t)I_{ex}(\xi). \tag{B4b}$$

Here, $s(t)$ and $k(t)$ contain all the kinetic factors in the scattering and the absorption, respectively. $I_{ex}(\xi)$ is the excitation intensity at point ξ in the sample. It is an instantaneous excitation at time $t = 0$. The excitation intensity can be written as

$$I_{ex}(\xi) = E_0 \exp[-\eta_{532}c_{bR}(l - \xi)]. \tag{B5}$$

We do not take into account the change of I_m and I_{ex} due to scattering, since this is a small perturbation. The differential equation describing the intensity of the monitor light, I_m is

$$\frac{\partial I_m}{\partial \xi} = -I_m[\eta^0_{325} + k(t)I_{ex}(\xi)]c_{bR}. \tag{B6}$$

The solution to Eq. B6 is

$$I_m(\xi, t) = I_0 \exp(A), \tag{B7}$$

where A is a function of c_{bR}, such that

$$A = -\eta^0_{325}c_{bR}\xi - k(t)E_0c_{bR} \cdot \exp(-\eta_{532}c_{bR}l)\left[\frac{\exp(\eta_{532}c_{bR}\xi) - 1}{\eta_{532}c_{bR}}\right]. \tag{B8}$$

We use Eqs. B7 and B8 in Eq. B2 and integrating over the entire volume of sample imaged upon the PMT, we obtain the following relation as the fractional scattering change

$$\frac{\Delta I_{sc}}{I_{sc}(t = 0)} = \frac{\int \{[1 + s(t)I_{ex}(\xi)] \exp[A - \eta_{325}(\xi, t)\rho c_{bR}] - \exp[-\eta^0_{325}c_{bR}(\xi + \rho)]\}\, dV}{\int \exp[-\eta^0_{325}c_{bR}(\xi + \rho)]\, dV}. \tag{B9}$$

This complicated equation can be more easily evaluated when the concentration of bR is small (as in these measurements). Expanding Eq. B9 to the first order terms and neglecting ηcl relative to unity, we obtain

$$\frac{\Delta I_{sc}}{I_{sc}} \approx s(t)E_0 - \frac{1}{2}k(t)E_0c_{bR}(l + w). \tag{B10}$$

Thus, we have shown the scattering to have two components. One component is a function of the cross-section changes, $s(t)$, and independent of the chromophore concentration. The second component is a function of the absorption changes, $k(t)$, and has a linear dependence on the chromophore concentration. We have assumed that ηcl is small. For the experiments reported here, $\eta = 2.303\epsilon \approx 100{,}000\ \text{cm}^{-1}\text{M}^{-1}$, $c \leq 5.0$ μM, and $l \leq 5$ mm. As shown by the linear dependence of the data in Fig. 3 *b*, the data are sufficiently well described by this first order approximation.

We thank Zsolt Dancsházy for the generous supply of purple membrane used in these experiments.

This work has been supported in part by grants from the Office of Naval Research, grant N00014-WR-24020, and the Strategic Defense Initiative Organization under the Medical Free Electron Laser program. The opinions and assertions contained in this paper are the private views of the authors and are not to be construed as reflecting the views of the Uniformed Services University of the Health Sciences or the Department of Defense.

Received for publication 6 October 1989 and in final form 2 May 1990.

REFERENCES

1. Oesterhelt, D., and W. Stoeckenius. 1973. Function of a new photoreceptor membrane. *Proc. Natl. Acad. Sci. USA.* 70:2853–2857.
2. Stoeckenius, W., R. H. Lozier, and R. A. Bogomolni. 1979. Bacteriorhodopsin and the purple membrane of *Halobacteria. Biochim. Biophys. Acta.* 505:215–278.
3. Stoeckenius, W., and R. H. Lozier. 1974. Light energy conversion in *Halobacterium halobium. J. Supramol. Struct.* 2:769–774.
4. Razi Naqvi, K., J. Gonzalez-Rodrigues, R. J. Cherry, and D. Chapman. 1973. Spectroscopic technique for studying protein rotation in membranes. *Nat. New Biol.* 255:249–251.
5. Cherry, R. J., U. Müller, and G. Schneider. 1977. Rotational diffusion of bacteriorhodopsin in lipid membranes. *FEBS (Fed. Eur. Biochem. Soc.) Lett.* 80:465–469.
6. Cherry, R. J., M. P. Heyn, and D. Oesterhelt. 1977. Rotational

diffusion and exciton coupling of bacteriorhodopsin in the cell membrane. *FEBS (Fed. Eur. Biochem. Soc.) Lett.* 78:25–30.

7. Sherman, W. V., and S. R. Caplan. 1977. Chromophore mobility in bacteriorhodopsin. *Nature (Lond.).* 265:273–274.
8. Korenstein, R., and B. Hess. 1978. Immobilization of bacteriorhodopsin and orientation of its transition moment in purple membrane. *FEBS (Fed. Eur. Biochem. Soc.) Lett.* 89:15–20.
9. Czégé, J., A. Dér, L. Zimányi, and L. Keszthelyi. 1982. Restriction of motion of protein side chains during the photocycle of bacteriorhodopsin. *Proc. Natl. Acad. Sci. USA.* 79:7273–7277.
10. Beece, D., S. F. Bowne, J. Czégé, L. Eisenstein, H. Frauenfelder, D. Good, M. C. Marden, J. Marque, P. Ormos, L. Reinisch, and K. T. Yue. 1981. The effect of viscosity on the photocycle of bacteriorhodopsin. *Photochem. Photobiol.* 33:517–522.
11. Keszthelyi, L., and P. Ormos. 1980. Electric signals associated with the photocycle of bacteriorhodopsin. *FEBS (Fed. Eur. Biochem. Soc.) Lett.* 109:189–193.
12. Czégé, J. 1987. Light scattering changes during the photocycle of bacteriorhodopsin. *Acta Biochim. Biophys. Hung.* 22:463–478.
13. Czégé, J. 1987. Bent membrane model of the purple membrane. Theoretical details and further experimental data. *Acta Biochim. Biophys. Hung.* 22:479–489.
14. Czégé, J. 1988. Light scattering changes and protein distortion in the bacteriorhodopsin during the photocycle. *FEBS (Fed. Eur. Biochem. Soc.) Lett.* 242:89–93.
15. Oesterhelt, D., and W. Stoeckenius. 1974. Biomembranes. *Methods Enzymol.* 31:667–668.
16. Becher, B., F. Tokunaga, and T. G. Ebrey. 1978. Ultraviolet and visible absorption spectra of purple membrane protein and photocycle intermediates. *Biochemistry.* 17:4923–4926.
17. Keszthelyi, L. 1980. Orientation of membrane fragments by electric field. *Biochim. Biophys. Acta.* 598:429–436.
18. Renthal, R., and C. H. Cha. 1984. Charge asymmetry of the purple membrane measured by uranyl quenching of dansyl fluorescence. *Biophys. J.* 45:1001–1006.
19. Blaurock, A. E. 1975. Bacteriorhodopsin: a trans-membrane pump containing α-helix. *J. Mol. Biol.* 93:139–158.
20. Tristram-Nagle, S., C.-P. Yang, and J. F. Nagle. 1986. Thermodynamic studies of purple membrane. *Biochim. Biophys. Acta.* 854:58–66.
21. Barabás, K., A. Dér, Zs. Dancsházy, P. Ormos, M. Marden, and L. Keszthelyi. 1983. Electro-optical measurements on aqueous suspension of purple membrane from *Halobacterium halobium. Biophys. J.* 43:5–11.
22. Arrio, B., G. Johannin, P. Volfin, M. Lefort-Tran, L. Packer, A. E. Robinson, and E. Hrabeta. 1986. Aggregation of proton release of purple and white membranes following cleavage of the carboxyl-terminal tail of bacteriorhodopsin. *Arch. Biochem. Biophys.* 246: 185–191.
23. Heyn, M. P., R. J. Cherry, and U. Müller. 1977. Transient and linear dichroism studies on bacteriorhodopsin: determination of the orientation of the 568 nm all-*trans* retinal chromophore. *J. Mol. Biol.* 117:607–620.
24. Keszthelyi, L. 1984. Intramolecular charge shifts during the photoreaction cycle of bacteriorhodopsin. *In* Information and Energy Transduction in Biological Membranes. C. L. Bolis, E. J. M. Helmreich, and H. Passow, editors. Alan R. Liss Inc., New York. 51–72.
25. Kerker, M. 1969. The Scattering of Light and Other Electromagnetic Radiation. Academic Press, Inc., New York.